10

TWO-DIMENSIONAL CRYSTALLOGRAPHY

E. Vlieg* and I. K. Robinson
AT&T Bell Laboratories, Murray Hill, New Jersey 07974, USA

10.1 Introduction

Surface Crystallography is a branch of crystallography that has blossomed since the arrival of synchrotron radiation. In some ways it is a simple extension of traditional three-dimensional crystallography, taking advantage of the increased flux to reduce the sample size requirement to its natural limit, the monolayer. Another point of view is that the field represents the analysis of diffuse scattering from systems that are highly correlated in two directions. It is in fact the confluence of both.

* Present address: FOM-Institute, Kruislaan 407, 1098 SJ Amsterdam, The Netherlands.

In this chapter we shall treat the problem from the former point of view, attempting to relate 2D crystallography to its 3D brother at all stages. There are special considerations needed throughout the application, at the level of sample preparation, data collection, data analysis and even the presentation of results. We shall not discuss sample preparation at any length, because this falls under surface and interface science. It suffices to say that 2D crystals do exist in nature. They appear at the surfaces of 3D crystals and frequently adopt structures that are subtly or dramatically different from the bulk, technically referred to as 'relaxation' and 'reconstruction' respectively. They appear at crystal-crystal, crystal-liquid and crystal-amorphous interfaces. These cases can be examined like pure surfaces by virtue of the penetrating property of X-rays; this statement often comes as a surprise to surface scientists, used to thinking about electron-based analytic techniques. Finally there are spontaneously forming 2D crystals associated with non-periodic interfaces such as gas-liquid (e.g. air-water). Surfactant molecules are found to self-assemble there under certain conditions. Biological membranes are sometimes found to contain organized arrays of protein molecules, which are also 2D crystals.

This chapter treats diffraction from 2D crystals from first principles, which serves to review the basis of all crystallography. As we shall see, the fundamental concept of integrated intensity needs modification from the 3D case. This change, as well as the strong anisotropy implicit in the 2D problem, means changes are needed in the data collection methods. It is found, for example, that a five- or six-circle diffractometer has advantages over the conventional four-circle machine, as discussed in Section 10.4.

One new concept which arises for surfaces as opposed to isolated monolayers is the construction of the Crystal Truncation Rod (CTR). This is necessary to explain how the diffraction from the surface overlaps that of the bulk and how the measurements switch smoothly from being bulk-sensitive to surface-sensitive. CTR measurements contain crystallographic information too, although they are found to require special handling, as discussed further below.

The history of the field is, like most fields benefiting from synchrotron radiation, exponentially growing in time. Surface effects have been observed very early on in the history of X-ray diffraction. CTRs were dealt with by Von

Laue's treatment of finite size effects in powder diffraction[1,2] and even acquire the name 'stacheln' there. The CTR is also manifested in the various treatments of stacking fault disorder in crystals.[3,4] Stacking faults are of course internal surfaces of crystals and must be handled analogously. Monolayer crystals have been studied as intercalation compounds, adsorbed films on powder substrates and liquid crystal films for many years.

Surface crystallography was first introduced in more or less its present incarnation by the work of Eisenberger and Marra,[5] who used surface science techniques to characterize a surface that they subsequently studied, under vacuum, with X-rays. This and other early work used rotating-anode sources, but these have been largely superseded by synchrotron sources, at which most of the experiments take place today. Surface science has also evolved dramatically during the same period, driven by high-technology applications. This not only has greatly facilitated the experiments (and the synchrotron machinery itself), but increased the interest in 2D crystallographic results, many of which have already found relevance in electronic devices, such as understanding the distribution of strain near to a semiconductor interface.

10.2 Kinematical diffraction theory

10.2.1 Derivation of the wave equation

In X-ray diffraction experiments a crystal is illuminated by an X-ray beam. By solving the Maxwell equations for this situation, the total electric field can be derived.[6] The alternating electric field of the incoming beam will induce an alternating polarization in the medium, which in turn gives rise to a scattered

---

1 M. von Laue, *Ann. der Physik* (folge V) **26**, 62 (1936).
2 R.W. James, *The Optical Principles of the Diffraction of X-Rays*. Cornell University Press (1955).
3 A. Guinier, *X-Ray Diffraction*, W.H. Freeman (1963).
4 H. Jagodzinski, *Acta Cryst.* **2**, 201 (1949).
5 P. Eisenberger and W. C. Marra, *Phys. Rev. Lett.* **46**, 1081 (1981).
6 M. Born and E. Wolf, *Principles of Optics*, 5th Ed., New York: Pergamon (1986).

beam. The quantity of interest is the intensity of the scattered beam. In the Maxwell equations the displacement can be written as

$$\mathbf{D} = \mathbf{E} + 4\pi\mathbf{P} = \varepsilon\mathbf{E} \qquad [10.1]$$

with $\mathbf{E}$ the electric field, $\mathbf{P}$ the polarization and $\varepsilon = 1 + 4\pi|\mathbf{P}|/|\mathbf{E}|$ the dielectric constant. The magnetic permeability μ is taken to be unity, so $\mathbf{H} = \mathbf{B}$. The following wave equation for the total electric field can then be derived from the Maxwell equations:

$$\nabla^2\mathbf{E}(\mathbf{r},t) = \frac{\varepsilon}{c^2}\frac{\partial^2}{\partial t^2}\mathbf{E}(\mathbf{r},t) \qquad [10.2]$$

with c the speed of light.

The vector nature of $\mathbf{E}$ will be ignored here; it can be accounted for by a polarization factor in the final result. We are interested in purely elastic scattering, and have to consider only one single frequency ω:

$$\mathbf{E}(\mathbf{r},t) = \mathbf{E}(\mathbf{r})e^{-i\omega t} \qquad [10.3]$$

Substitution of [10.3] into [10.2] yields

$$(\nabla^2 + k^2)\,\mathbf{E}(\mathbf{r}) = 0 \qquad [10.4]$$

with $k = \varepsilon\omega^2/c^2$. The dielectric constant is derived by considering a free electron in the electric field given by [10.3]. The equation of motion is

$$m\frac{\partial^2 x}{\partial t^2} = -eEe^{-i\omega t} \qquad [10.5]$$

with m the electron mass.

The solution of this equation of motion is

$$x = \frac{eE}{m\omega^2}\,e^{-i\omega t} \qquad [10.6]$$

The dipole moment due to the displacement of the single electron is -ex. For a system with electron density $\rho(\mathbf{r})$ the polarization then becomes

$$P = -e\rho(\mathbf{r})x = -\frac{e^2\rho(\mathbf{r})}{m\omega^2}\,Ee^{-i\omega t} \qquad [10.7]$$

and, using [10.1],

$$\varepsilon = 1 - \frac{4\pi e^2}{m\omega^2}\,\rho(\mathbf{r}) \qquad [10.8]$$

From [10.4] and [10.8] we arrive at

$$\left[\nabla^2 + k_0^2 - 4\pi r_e\rho(\mathbf{r})\right]\mathbf{E}(\mathbf{r}) = 0 \qquad [10.9]$$

with $k_0 = \omega/c = 2\pi/\lambda$ and $r_e = e^2/mc^2$ the classical electron radius. This is the fundamental wave equation to be solved.

10.2.2 Single-scattering approximation

In order to find the solution of the differential equation [10.9], it is useful to rewrite it as an equivalent integral equation by making use of the Green function $\mathbf{G}(\mathbf{r},\mathbf{r}')$:

$$\mathbf{E}(\mathbf{r}) = \mathbf{E}_i(\mathbf{r}) - 4\pi r_e\int\mathbf{G}(\mathbf{r},\mathbf{r}')\rho(\mathbf{r}')\mathbf{E}(\mathbf{r}')\,d\mathbf{r}' \qquad [10.10a]$$

where $\mathbf{E}_i(\mathbf{r})$ is the electric field of the incoming beam.

The appropriate form of the Green's function is[7]

$$G(\mathbf{r},\mathbf{r}') = \frac{e^{-ik|\mathbf{r}-\mathbf{r}'|}}{4\pi|\mathbf{r}-\mathbf{r}'|} \qquad [10.10b]$$

where k is the wave vector of the scattered beam.

X-rays are scattered only very weakly. For small crystals (or a surface) the amplitude of the scattered wave is much less than the incident wave amplitude. Therefore the first Born or single-scattering approximation is used: the total electric field $E(\mathbf{r}')$ in the integral is replaced by the incoming wave field $E_i(\mathbf{r})$. This approximation is known as the kinematical theory for X-ray diffraction. The incoming beam is assumed to be a plane wave:

$$E_i(\mathbf{r}) = E_0\, e^{-i\mathbf{k}_0\cdot\mathbf{r}} \qquad [10.11]$$

Then [10.10a] becomes

$$E_i(\mathbf{r}) + E_s(\mathbf{r}) = E_0\, e^{-i\mathbf{k}_0\cdot\mathbf{r}} - r_e E_0 \int \frac{e^{-ik|\mathbf{r}-\mathbf{r}'|}}{|\mathbf{r}-\mathbf{r}'|}\,\rho(\mathbf{r}')\, e^{-i\mathbf{k}_0\cdot\mathbf{r}'}\, d\mathbf{r}' \qquad [10.12]$$

The point of observation will be at a distance large compared with the dimensions of the scattering source. Then we obtain for the scattered beam

$$E_s(\mathbf{r}) = -E_0 \frac{e^{-ikr}}{r}\, g(\mathbf{Q}) \qquad [10.13]$$

with $\mathbf{Q} = \mathbf{k} - \mathbf{k}_0$ the momentum transfer (with magnitude $(4\pi \sin\theta)/\lambda$), and with the scattering amplitude $g(\mathbf{Q})$ defined as

$$g(\mathbf{Q}) = r_e \int \rho(\mathbf{r}) e^{i\mathbf{Q}\cdot\mathbf{r}}\, d\mathbf{r} \qquad [10.14]$$

[7] J.D. Jackson, *Classical Electrodynamics*, 2nd Edn., Wiley (1975).

10.2.3 Scattering from a bulk crystal

In order to evaluate the scattering amplitude, [10.14], an expression has to be derived for the electron density in the crystal $\rho(\mathbf{r})$. Let $\mathbf{a}_1$, $\mathbf{a}_2$ and $\mathbf{a}_3$ be the lattice parameters of the crystal. The electron density consists of the electron density in one unit cell, $\rho_u(\mathbf{r})$, repeated at all possible lattice vectors. It is convenient to use a convolution to express this. The convolution of two functions is defined as

$$f(\mathbf{r}) * g(\mathbf{r}) = \int f(\mathbf{r}')g(\mathbf{r}-\mathbf{r}')\, d\mathbf{r}' \qquad [10.15]$$

The electron density in the crystal can then be written as the convolution of $\rho_u(\mathbf{r})$ with all the lattice points:

$$\rho(\mathbf{r}) = \left[\rho_u(\mathbf{r}) * \sum_{m_1 m_2 m_3} \delta(\mathbf{r}-\mathbf{R})\right] s(\mathbf{r}) \qquad [10.16]$$

where $\mathbf{R} = m_1\mathbf{a}_1 + m_2\mathbf{a}_2 + m_3\mathbf{a}_3$ (with m_i integer) is a lattice vector, and where $s(\mathbf{r})$ is the crystal shape function. The value of $s(\mathbf{r})$ is 1 if $\mathbf{r}$ is within the crystal and 0 outside. Substitution of [10.16] into [10.14] gives

$$g(\mathbf{Q}) = \frac{r_e}{8\pi^3}\left[F(\mathbf{Q}) \sum_{m_1 m_2 m_3} \int \delta(\mathbf{r}-\mathbf{R}) e^{i\mathbf{Q}\cdot\mathbf{r}}\, d\mathbf{r}\right] * S(\mathbf{Q}) \qquad [10.17a]$$

with

$$F(\mathbf{Q}) = \int \rho_u(\mathbf{r}) e^{i\mathbf{Q}\cdot\mathbf{r}}\, d\mathbf{r} \qquad [10.17b]$$

and

$$S(\mathbf{Q}) = \int s(\mathbf{r}) e^{i\mathbf{Q}\cdot\mathbf{r}}\, d\mathbf{r} \qquad [10.17c]$$

In order to arrive at [10.17a], the multiplication theorem and the convolution theorem have been used. The summation in [10.17a] is evaluated as follows:

$$\sum_{m_1m_2m_3} \int \delta(\mathbf{r}-\mathbf{R})\, e^{i\mathbf{Q}\cdot\mathbf{r}}\, d\mathbf{r} = \sum_{m_1m_2m_3} e^{i\mathbf{Q}\cdot\mathbf{R}} = \begin{cases} \infty & \text{for } \mathbf{Q}\cdot\mathbf{R} = 2n\pi \\ 0 & \text{otherwise} \end{cases} \qquad [10.18]$$

The condition $\mathbf{Q}\cdot\mathbf{R} = 2n\pi$ is satisfied if

$$\mathbf{Q} = 2\pi\mathbf{H} \qquad [10.19a]$$

with

$$\mathbf{H} = h\mathbf{b}_1+k\mathbf{b}_2+l\mathbf{b}_3 \qquad [10.19b]$$

where the $\mathbf{b}_i$ are defined by

$$\mathbf{a}_i\cdot\mathbf{b}_j = \delta_{ij} \qquad [10.19c]$$

Thus the $\mathbf{b}_i$ are the reciprocal lattice parameters and h, k and l the Miller indices. From [10.19] it follows that

$$\begin{aligned} \mathbf{Q}\cdot\mathbf{a}_1 &= 2\pi h \\ \mathbf{Q}\cdot\mathbf{a}_2 &= 2\pi k \\ \mathbf{Q}\cdot\mathbf{a}_3 &= 2\pi l \end{aligned} \qquad [10.20]$$

These are the well-known 'Laue conditions' for diffraction. They show that diffraction from a bulk crystal only occurs at points (hk$l$) in reciprocal space.

The summation in [10.18] can be written as

$$\sum_{m_1m_2m_3} e^{-i\mathbf{Q}\cdot\mathbf{R}} = \frac{8\pi^3}{V_u}\sum_{hkl} \delta(\mathbf{Q}-2\pi\mathbf{H}) \qquad [10.21]$$

with $V_u = (\mathbf{a}_1\times\mathbf{a}_2)\cdot\mathbf{a}_3$ the unit-cell volume. Using this in [10.17a], the

scattering amplitude becomes

$$\begin{aligned} g(\mathbf{Q}) &= \frac{r_e}{V_u}\left[\sum_{hkl} F(\mathbf{Q})\delta(\mathbf{Q}-2\pi\mathbf{H})\right] * S(\mathbf{Q}) \\ &= \frac{r_e}{V_u}\sum_{hkl} F_{hkl}\, S(\mathbf{Q}-2\pi\mathbf{H}) \end{aligned} \qquad [10.22a]$$

$$\text{with } F_{hkl} = \int \rho_u(\mathbf{r})\, e^{2\pi i\mathbf{H}\cdot\mathbf{r}}\, d\mathbf{r}) \qquad [10.22b]$$

F_{hkl} is the structure factor; it is $F(\mathbf{Q})$, [10.17b], evaluated at the reciprocal lattice point (hk$l$).

The structure factor is the Fourier transform of the electron density in the unit cell. An expression more convenient than [10.22b] can be derived for the structure factor, when it is assumed that the electron density in the unit cell is the summation of the electron densities for the individual atoms:

$$\rho_u(\mathbf{r}) = \sum_j \rho_j(\mathbf{r}) * \delta(\mathbf{r}-\mathbf{r}_j) \qquad [10.23]$$

$\rho_j(\mathbf{r})$ is the electron density of atom j centered at $\mathbf{r} = \mathbf{r}_j$. Then

$$F_{hkl} = \sum_j f_j\, e^{2\pi i\mathbf{H}\cdot\mathbf{r}_j} \qquad [10.24a]$$

$$\text{with } f_j(\mathbf{Q}) = \int \rho_j(\mathbf{r})\, e^{-i\mathbf{Q}\cdot\mathbf{r}}\, d\mathbf{r}) \qquad [10.24b]$$

the atomic scattering factor.

When the position of an atom in the unit cell is given in fractional coordinates $\mathbf{r}_j = x_j\mathbf{a}_1+y_j\mathbf{a}_2+z_j\mathbf{a}_3$, we obtain

$$F_{hkl} = \sum_j f_j\, e^{2\pi i(hx_j+ky_j+lz_j)} \qquad [10.25]$$

In deriving the scattering amplitude, the electrons in the crystal were assumed to be free. This is a simplification of the situation in a crystal, where the electrons are bound. If the X-ray frequency is near a resonant frequency for some of the electrons and also if absorption is present, the polarization can no longer be described by the simple expression in [10.8], which was derived for a free electron. These changes in the polarization are taken into account by considering the atomic scattering factors as complex and wavelength-dependent. Thus the atomic scattering factor in [10.25] is written as

$$f = f_0 + f' + if'' \qquad [10.26]$$

where f_0 is independent of the wavelength, as discussed in detail in Chapter 6.

Until now it was assumed that the atoms are fixed at definite positions in the crystal. However, the atoms will vibrate thermally about their equilibrium positions. This gives rise to thermal diffuse scattering, which is present as a 'background' in reciprocal space. Because part of the scattered intensity 'disappears' into the diffuse scattering, the intensity of the diffraction peaks will decrease. This is conveniently described by the Debye-Waller factor[8,9] in the structure factor:

$$F_{hkl} = \sum_j f_j \, e^{-B_j Q^2/(16\pi^2)} \, e^{2\pi i(hx_j + ky_j + lz_j)} \qquad [10.27]$$

The Debye-Waller parameter B is related to the mean-square thermal vibration amplitude $\langle u^2 \rangle$ by

$$B = 8\pi^2 \langle u^2 \rangle \qquad [10.28]$$

Here B is assumed to be isotropic. More generally, B can be written as a tensor and the component along the direction of the momentum transfer should be

8 P. Debye, *Ann. der Physik* **45**, 49 (1914).
9 B.E. Warren, *X-Ray Diffraction*, Reading, MA: Addison-Wesley (1969).

used in the Debye-Waller factor (see Chapter 5). The structure factor as written in [10.27] is the form used in fitting a structure model to experimental data.

Using the equations derived above, we can rewrite [10.14] for the scattering amplitude as

$$g(hkl) = r_e \sum_{m}^{\text{all unit cells}} F_{hkl} \, e^{2\pi i \mathbf{H}\cdot\mathbf{R}_m} \qquad [10.29]$$

with $\mathbf{R}_m$ pointing to the origin of unit cell m. This expression may be a more intuitive start in evaluating the scattering amplitude than the equivalent expression [10.22a].

10.3 Surface X-ray diffraction

10.3.1 Reconstructed surfaces

In the previous section the scattering amplitude from a bulk crystal was derived. Now we turn our attention to diffraction from a surface. Here a surface is considered to be the top few layers of a crystal. Atoms in the surface may be displaced from bulk positions or different atom types may be present. The special case of diffraction from a surface is straightforwardly derived from the bulk equations. The difference with a bulk crystal is that the surface unit cell is repeated only in the x and y directions, and not in the z direction ($\mathbf{a}_1$ and $\mathbf{a}_2$ are the in-plane lattice parameters). The unit cell itself may extend over several layers in the z direction. Because for a surface there is no periodicity in the perpendicular direction, the Laue condition in that direction is relaxed, which means that the Miller index l is no longer required to be integer but may assume any value. Thus diffraction from a surface does not occur in points in reciprocal space, but rather in rods.

Instead of [10.16] for the electron density in a bulk crystal, we obtain for a surface

$$\rho_S(\mathbf{r}) = \left[\rho_u(\mathbf{r}) * \sum_{m_1 m_2} \delta(x-m_1a_1, y-m_2a_2)\right] s(x,y) \qquad [10.30]$$

In analogy with [10.22a], the following expression is then obtained for the scattering amplitude:

$$g_S(\mathbf{Q}) = \frac{r_e}{A_u} \sum_{hk} F^S_{hkl}\, S(q_x-2\pi b_1 h,\, q_y-2\pi b_2 k) \qquad [10.31]$$

where $A_u = |\mathbf{a}_1 \times \mathbf{a}_2|$ is the unit-cell area.

In general, the total scattering amplitude will be the sum of the contributions from both the surface and the bulk. If the surface is reconstructed, the surface unit cell is larger than the unit cell of the bulk lattice, and diffraction peaks occur at positions in reciprocal space that are not allowed for the bulk crystal. At these positions [10.31] gives the correct result for the total scattering amplitude.

There are two equivalent ways of labeling reflections from a reconstructed surface. The first is to use the lattice parameters of the bulk lattice, and to label the reflections by non-integer values of h and k (fractional-order reflections). The second way is to define new lattice vectors corresponding to the new unit cell. Then the reflections are labeled by integer values for h and k. The first notation has the advantage that reflections from the reconstructed surface are clearly identified by the non-integer values of the Miller indices, and is therefore the one commonly used in the literature.

10.3.2 Crystal truncation rods

At positions in reciprocal space where the bulk is not forbidden, the total signal will be the sum of the bulk and surface contributions. Before considering this sum, however, it is instructive to look more closely at the bulk contribution itself. The bulk scattering amplitude was given in [10.22a], and

we concluded that diffraction occurs only at points in reciprocal space, given by the Miller indices (hk*l*). This is not entirely true, because a Bragg spot will in general have a profile that is determined by the Fourier transform of the crystal shape function, with possible additional broadening due to mosaic spread. In the case of diffraction from a flat crystal the effective shape of the crystal is determined by the fact that the incoming beam is attenuated as a function of depth. The shape function in the perpendicular direction therefore has a step shape at the crystal boundary, and a smooth decay as a function of depth. In the parallel direction we may assume that a rectangle is illuminated. The crystal shape function is therefore given by

$$S(\mathbf{r}) = \begin{cases} e^{z/\mu} & |x| \le L_x/2;\ |y| \le L_y/2;\ z \le 0 \\ 0 & \text{otherwise} \end{cases} \qquad [10.32]$$

where μ is the penetration depth, and L_x and L_y are the illuminated lengths of the crystal in the x- and y-directions respectively. For simplicity, an orthogonal lattice is assumed. The Fourier transform of the crystal shape function is then found to be

$$\begin{aligned} S(\mathbf{Q}) &= \int_{-L_x/2}^{L_x/2} e^{-iq_1x}\,dx \int_{-L_y/2}^{L_y/2} e^{-iq_2y}\,dy \int_{-\infty}^{0} e^{-iq_3z} e^{z/\mu}\,dz \\ &= \frac{\sin(L_xq_x/2)}{q_x/2} \frac{\sin(L_yq_y/2)}{q_y/2} \frac{1}{-iq_z+1/\mu} \end{aligned} \qquad [10.33]$$

Ignoring the $1/\mu$ term (i.e. assuming infinite penetration depth), the scattering amplitude is

$$g(\mathbf{Q}) = \frac{r_e}{V_u} \sum_{hkl} F^B_{hkl} \frac{\sin[L_x(q_x-2\pi b_1 h)/2]}{(q_x-2\pi b_1 h)/2} \frac{\sin[L_y(q_y-2\pi b_2 k)/2]}{(q_y-2\pi b_2 k)/2} \times \frac{1}{-i(q_z-2\pi b_3 l)} \qquad [10.34]$$

Thus we see that the scattering amplitude around each Bragg point is sharp in the $\mathbf{q}_x$ and $\mathbf{q}_y$ directions, but drops off as $1/q_z$ in the direction perpendicular to the surface.[10,11] The intensity (proportional to the square of the scattering amplitude) will drop off as $1/q_z^2$.

In order to derive the exact total scattering amplitude, the summation over (hk$l$) has to be carried out. Since the Bragg peaks are generally very sharp in the $\mathbf{q}_x$ and $\mathbf{q}_y$ directions one term in the summation over h and k is sufficient. This is not true in the perpendicular direction. It is possible, but rather tedious, to do this summation over l analytically using [10.34].[12] For simplicity we shall use the equivalent form for the scattering amplitude as given in [10.29], which gives for the summation in the perpendicular direction

$$\sum_{n_3=-\infty}^{0} e^{-2\pi i l n_3}\, e^{a_3 n_3/\mu} = \frac{1}{1-e^{-2\pi i l}\, e^{-a_3/\mu}} \equiv \eta_{CTR} \qquad [10.35]$$

This is the effective enhancement factor of the scattering from a unit cell due to the 3D periodicity of the bulk. Absorption is only important near Bragg peaks. Since we are here interested in surface diffraction, we shall not evaluate the scattering amplitude near Bragg peaks, and therefore may ignore the absorption. Then the amplitude of η_{CTR} is

$$|\eta_{CTR}| = \frac{1}{2\,\sin(\pi l)} \qquad [10.36]$$

Thus the bulk still peaks at integer values of l, but there is also intensity for other values of l. In the direction perpendicular to the surface, all Bragg peaks are connected by rods, these are the crystal-truncation rods.[12] Close to integer values of l the amplitude drops off as $1/q_z$, the same result as [10.34], but by carrying out the summation over l we also have obtained the correct answer for l-values in between two Bragg peaks.

10 S.R. Andrews and R.A. Cowley, *J. Phys.* **C18**, 6427 (1985).
11 I.K. Robinson, *Phys. Rev.* **B33**, 3830 (1986).
12 H. You, in Proceedings of 2nd International Conference on Surface X-Ray and Neutron Scattering, Bad Honnef, Germany, H. Zabel and I.K. Robinson, Eds., Berlin: Springer, to be published (1991).

Replacing the summation over l by η_{CTR}, we may now write for the scattering amplitude from the bulk

$$g_B(\mathbf{Q}) = \frac{r_e}{A_u} \sum_{hk} F^B_{hkl}\, \eta_{CTR}\, S(q_x - 2\pi b_1 h,\, q_y - 2\pi b_2 k) \qquad [10.37]$$

The total scattering amplitude is now simply obtained by taking the sum of the surface and bulk contributions:

$$g(\mathbf{Q}) = \frac{r_e}{A_u} \sum_{hk} (F^S_{hkl} + F^B_{hkl}\, \eta_{CTR})\, S(q_x - 2\pi b_1 h,\, q_y - 2\pi b_2 k) \qquad [10.38]$$

In the case of a reconstructed surface the bulk contribution at the fractional-order positions in reciprocal space is zero, and [10.38] reduces to the simpler form in [10.31]. If the surface is not reconstructed, the positions of the surface can still be different from those of the bulk, e.g. the surface atoms may be displaced inward. Such a rearrangement that does not involve a change of the surface unit cell is called relaxation. The effect of such a relaxation can be calculated by including the displaced surface atoms in the F^S_{hkl} term of [10.38].

The assumption that the crystal is a rectangle with all unit cells perfectly lined up is not valid in general. Possible types of disorder are antiphase domains on a reconstructed surface, or roughness in the form of steps and islands. Such disorder will lead to a broadening of the diffraction profiles. In fact, the accurate measurement of diffraction profiles enables a detailed analysis of the disorder at a surface.[13] If one is interested in the unit cell structure, the results derived here are valid as long as the integrated intensity, discussed in the following section, is measured.[14]

13 M.G. Lagally, D.E. Savage, M.C. Trinigides, in *Reflection High-Energy Electron Diffraction and Reflection Electron Imaging of Surfaces*, P.K. Larsen and P.J. Dobson, Eds., New York: Plenum (1988), p. 163.
14 E. Vlieg, J.F. van der Veen, S.J. Gurman, C. Norris and J.E. Macdonald, *Surf. Sci.* **210**, 301 (1989).

10.3.3 Integrated intensity

The scattered intensity is given by $I = (8\pi/c)E_S E_S^*$. In the usual situation the diffraction peaks are very narrow and do not overlap, and only one term in the summation over hk is important in [10.38]. From [10.13] and [10.38] the scattered intensity is obtained:

$$I(\mathbf{Q}) = \frac{I_0}{r^2}\left(\frac{r_e}{A_u}\right)^2 |F_{hkl}|^2 \, S^2(q_x - 2\pi b_1 h,\, q_y - 2\pi b_2 k) \qquad [10.39]$$

where

$$|F_{hkl}| = |F^S_{hkl} + F^B_{hkl}\,\eta_{CTR}| \qquad [10.40]$$

and $I_0 = (8\pi/c)E_0 E_0^*$ the incident flux. Using the Fourier transform of the crystal shape function as given in [10.33], the scattered intensity is

$$I(\mathbf{Q}) = \frac{I_0}{r^2} r_e^2 |F_{hkl}|^2 \frac{\sin^2(\pi h L_x/a_1)}{\pi^2 h^2} \frac{\sin^2(\pi k L_y/a_2)}{\pi^2 k^2} \qquad [10.41]$$

A more easily accessible and well-defined quantity that can be accurately measured is the integrated intensity.[9] In principle, the integrated intensity is obtained by scanning around the reflection of interest over the complete region in reciprocal space where intensity is present. In the type of experiments discussed here this is done by rotating the crystal and using a detector with a large enough angular acceptance.

In order to derive the integrated intensity, we first write down the differential scattering cross-section

$$\frac{d\sigma}{d\Omega} = r_e^2 |F_{hkl}|^2 \frac{\sin^2(\pi h L_x/a_1)}{\pi^2 h^2} \frac{\sin^2(\pi k L_y/a_2)}{\pi^2 k^2} \qquad [10.42]$$

In Fig. 10.1 a typical experimental geometry is shown, in both real and reciprocal space. The angle of incidence is β and the outgoing angle is β'. The projection of the scattering angle onto the surface is denoted here by $2\theta'$. It is the 2D character of the surface that gives rise to the diffraction rods in reciprocal space. When measuring the integrated intensity, the crystal is rotated with an angular velocity ω about the surface normal. As shown schematically in Fig. 10.2, the detector accepts the radiation over an interval $\Delta\psi$ along the in-plane direction (Fig. 10.2a) and over $\Delta\gamma$ in the perpendicular direction (Fig. 10.2c). Diffraction occurs when the Ewald sphere (defining elastic scattering) intersects a diffraction rod. The total intensity is obtained by integrating the instantaneous intensity over time and over the acceptance of the detector:

$$I_{int} = \int I_0 \frac{d\sigma}{d\Omega}\, dt\, d\psi\, d\gamma = \frac{I_0}{\omega}\int \frac{d\sigma}{d\Omega}\, d\alpha\, d\psi\, d\gamma \qquad [10.43]$$

where $d\alpha$ is the rotation angle of the crystal in time dt. The angles τ_1 and τ_2 (Fig. 10.2a) are defined such that $\tau_1 + \tau_2 = 2\theta'$. From Fig. 10.2(b) it is seen that the integration over $d\alpha$ and $d\psi$ corresponds to an integration over an area element

$$dA = k q_{||} \cos\tau_1\, d\alpha\, d\psi \qquad [10.44]$$

This element can also be expressed in terms of the in-plane Miller indices. Using $\mathbf{q}_{||} = 2\pi(\mathbf{b}_1 h + \mathbf{b}_2 k)$ (with h and k in this case *continuous* parameters) we get

$$dA = \frac{4\pi^2}{A_u}\, dh\, dk \qquad [10.45]$$

Thus

$$d\alpha\, d\psi = \frac{4\pi^2}{A_u}\frac{1}{k q_{||} \cos\tau_1}\, dh\, dk = \frac{\lambda^2}{A_u} L\, dh\, dk \qquad [10.46]$$

where $L = k/(q_{||}\cos\tau_1)$ is the Lorentz factor. Substituting this and [10.34] in

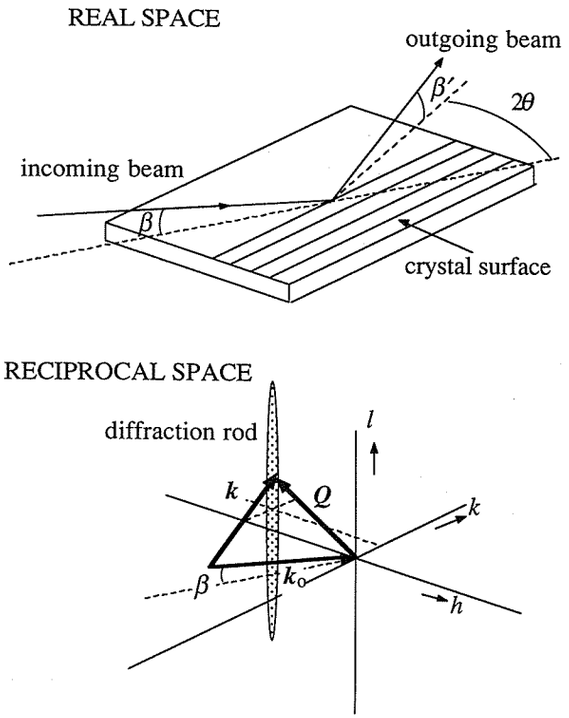

Fig. 10.1. Schematic of a typical X-ray diffraction geometry. (a) The situation in real space, where the angle of incidence is *b* and the outgoing angle is *b'*. In surface diffraction, the beam is scattered over an in-plane angle 2*q* by strings of atoms in the surface. (b) The situation in reciprocal space. The incoming beam is represented by the wave vector $\mathbf{k}_0$, the outgoing beam by $\mathbf{k}$ and the momentum transfer by $\mathbf{Q}$. In surface X-ray diffraction, scattering occurs for $\mathbf{Q}$ pointing to rods in reciprocal space.

[10.43], we get for the integrated intensity

$$I_{int} = r_e^2 \frac{I_0}{\omega} \frac{\lambda^2}{A_u} L \int \frac{\sin^2(\pi h L_x/a_1)}{\pi^2 h^2 \ dh} \int \frac{\sin^2(\pi k L_y/a_2)}{\pi^2 k^2 \ dk} \int |F_{hkl}|^2 \, d\gamma \qquad [10.47]$$

The integration over dh and dk is standard. In order to get a meaningful

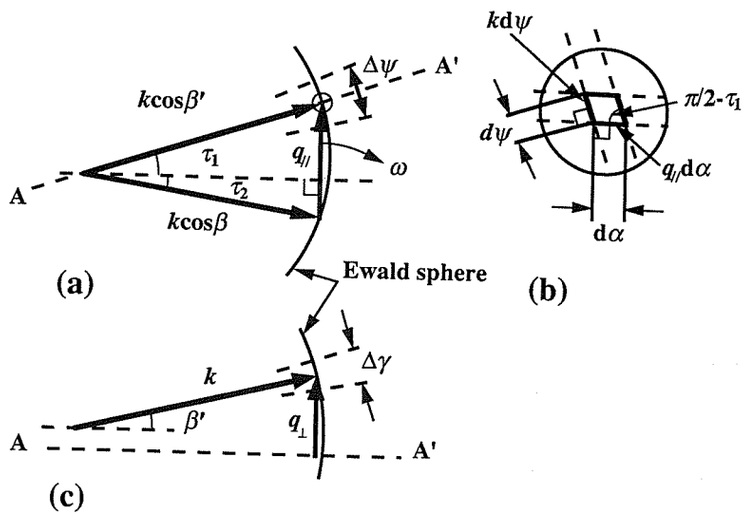

Fig. 10.2. Geometry used for deriving the integrated intensity of a reflection. (a) A projected top view, where the opening angle of the detector in the in-plane direction is indicated by Δψ. (b) Detail of (a), showing the area element over which the intensity is integrated when rotating the crystal. (c) Cross-sectional view along the line AA' of (a). The angular acceptance of the detector in the perpendicular direction is Δγ.

integrated intensity, the detector acceptance Δγ should be chosen sufficiently small to assure that $|F_{hkl}|$ is nearly constant. Then

$$I_{int} = r_e^2 \frac{I_0}{\omega} \frac{\lambda^2}{A_u} L \frac{L_x}{a_1} \frac{L_y}{a_2} |F_{hkl}|^2 \Delta\gamma$$

$$= r_e^2 \frac{I_0}{\omega} \frac{\lambda^2 A}{A_u^2} L \ |F_{hkl}|^2 \Delta\gamma \qquad [10.48a]$$

where A is the illuminated surface area. Including the polarization factor P, discussed in Chapter 4, in the integrated intensity, we get

$$I_{int} = r_e^2 \frac{I_0}{\omega} \frac{\lambda^2 A}{A_u^2} L \, P \, |F_{hkl}|^2 \Delta\gamma \qquad [10.48b]$$

The integrated intensity corresponds to a slice of a diffraction rod at a particular l-value.

The derivation of the Lorentz factor is simplified if it is assumed that $\beta = \beta'$. From Fig. 10.2(a), it is then found that $\tau_1 = \tau_2 = \theta'$ and $q_{\parallel} = 2k \cos\beta \sin\theta'$, which gives

$$L = \frac{k}{2k \cos\beta \sin\theta \cos\theta'} = \frac{1}{\cos\beta \sin 2\theta'} \qquad [10.49]$$

For $\beta = 0$ (where $2\theta' = 2\theta$) this reduces to the familiar result of $\sin^{-1} 2\theta$. The general case with $\beta \neq \beta'$ requires a more detailed evaluation of L.

10.3.4 Structure analysis

From the measured integrated intensity the square of the structure factor, $|F_{hkl}|^2$, can be derived. A list of experimentally determined structure factors can be compared directly with a theoretical structure model by using the theoretical formula [10.27] for the structure factor. The structure of the surface is found from an optimization of the structure-model parameters using a least-squares minimization of $\chi^2 = \Sigma(F_{obs}-|F_{calc}|)^2/\sigma^2_{obs}$ where σ^2_{obs} is the experimental standard deviation of the observation.[15]

X-ray diffraction data yield also model-independent information, as will now be shown. By taking the inverse Fourier transform of the expressions for $g(\mathbf{Q})$ as given in [10.14] and [10.22a], the electron density in a bulk crystal can be expressed as

$$\rho(\mathbf{r}) = \frac{1}{V_u} \sum_{hkl} F_{hkl} e^{-2\pi i \mathbf{H}\cdot\mathbf{r}}\, s(\mathbf{r}) \qquad [10.50]$$

with the reciprocal vector $\mathbf{H}$ defined by [10.19b]. Thus the electron density can be written as a Fourier series expansion with the structure factors as coefficients. From the structure factor [10.27] it is seen that a measurement at

[15] P.R. Bevington, *Data Reduction and Error Analysis for the Physical Sciences, New York:* McGraw-Hill (1969).

$l = 0$ is insensitive to the z-position of the atoms in the unit cell, and therefore yields the z-projected electron density. In the case of *surface* diffraction the projected electron density is

$$\rho(x,y) = \frac{1}{A_u} \sum_{hk} F_{hk0} e^{-2\pi i \mathbf{H}\cdot\mathbf{r}}\, s(x,y) \qquad [10.51]$$

It is not possible to measure the electron density directly, because experimentally only the *amplitude* of the structure factor is determined, whereas the expansion of ρ requires also the phase. This is known as the *phase problem.*

A function that can directly be obtained from the experimental data and yields model-independent information is the Patterson function. The Patterson function $P(\mathbf{r})$ is defined[9,16] as

$$P(\mathbf{r}) = \int_{\text{unit cell}} \rho(\mathbf{r}')\rho(\mathbf{r}+\mathbf{r}')\, d\mathbf{r}' \qquad [10.52]$$

The Patterson function is the autocorrelation function of the electron density and it shows peaks for $\mathbf{r}$ equal to an interatomic vector.

In order to derive a convenient expression for $P(\mathbf{r})$, [10.50] is substituted in [10.52]. Since the integral extends over only one unit cell, the crystal shape function $s(\mathbf{r}) = 1$, and the Patterson function becomes

$$P(\mathbf{r}) = \frac{1}{V_u^2} \int \sum_{hkl} \sum_{h'k'l'} F_{hkl}\, F_{h'k'l'}\, e^{-2\pi i \mathbf{H}'\cdot\mathbf{r}}\, e^{-2\pi i (\mathbf{H}+\mathbf{H}')\cdot\mathbf{R}}\, d\mathbf{R} \qquad [10.53]$$

Using the definition of the δ-function, this can be written as

$$P(\mathbf{r}) = \frac{1}{V_u} \sum_{hkl} F_{hkl}\, F_{\overline{hkl}}\, e^{-2\pi i \mathbf{H}\cdot\mathbf{r}} \qquad [10.54]$$

[16] A.L. Patterson, *Phys. Rev.* **46**, 372 (1934).

Taking the summation terms for (hk$l$) and ($\overline{hkl}$) together and using $F^*_{hkl} = F_{\overline{hkl}}$, this becomes

$$P(\mathbf{r}) = \frac{1}{V_u}\sum_{hkl} |F_{hkl}|^2 \cos(2\pi\mathbf{H}\cdot\mathbf{r}) \qquad [10.55]$$

The analogous 2D Patterson function for surface X-ray diffraction is obtained with the $l = 0$ values of the structure factors:

$$P(x,y) = \frac{1}{A_u}\sum_{hk} |F_{hk0}|^2 \cos(2\pi\mathbf{H}\cdot\mathbf{r}) \qquad [10.56]$$

Thus the Patterson function can be computed directly from the experimental data. It gives the interatomic vectors in the unit cell, and is therefore a useful tool in deriving the structure of a unit cell. Since the $l = 0$, 2D section of the data are used, the resulting real-space function is a 2D projection of the surface onto a plane.

As mentioned above, the electron density can only be determined from the data if the phases of the structure factors are known. If we have a model that describes the data reasonably well then we may assume that the phase factors of the model are approximately those of the data. This allows the calculation of the difference in electron density between the model and the data. Write the structure factor as

$$F_{hkl} = |F_{hkl}|e^{-i\phi_{hkl}} \qquad [10.57]$$

Taking the summation terms for (hk) and ($\overline{hk}$) together in [10.51], we get for the projected electron density

$$\rho(x,y) = \frac{1}{A_u}\sum_{h,k} |F_{hk0}| \cos(2\pi\mathbf{H}\cdot\mathbf{r} - \phi_{hk0})\, s(x,y) \qquad [10.58a]$$

Assuming that the actual phase factor is close to the one calculated for the model

structure, we then find for the electron density difference

$$\Delta\rho(x,y) = \frac{1}{A_u}\sum_{h,k} (|F^{dat}_{hk0}| - |F^{model}_{hk0}|) \cos(2\pi\mathbf{H}\cdot\mathbf{r} - \phi^{model}_{hk0})\, s(x,y) \qquad [10.58b]$$

A contour plot of this function is a valuable tool in a structure analysis: positive peaks indicate a missing atom at that position, whereas negative peaks show that the model contains rather too many (or too heavy) atoms.

10.4 Experimental equipment

The technique of surface X-ray diffraction requires the combination of an accurate diffractometer with a surface science vacuum chamber. Synchrotron radiation is highly polarized in the horizontal plane. Consequently, in order to avoid near-zero polarization factors for scattering angles of about 90°, it is necessary that the sample surface be mounted vertically, and hence that the main axis of the diffractometer be horizontal. There are various possibilities to make equipment according to these requirements.

A relatively easy approach is to have a small transfer cell ('baby chamber') that can either be mounted onto a diffractometer or attached to a vacuum chamber (via a valve).[17,18] An approach that allows for heavier and more sophisticated vacuum chambers is a 'z-axis'-type diffractometer,[19] but also in this case the entire vacuum chamber has to be rotated in order to rotate the sample.

Fuoss and Robinson[20] introduced the idea to use a differentially pumped rotary feedthrough for the coupling of the diffractometer motions to the sample in vacuum. In that case the weight of the vacuum chamber is not limited by the maximum load that the diffractometer can take, and much more sophisticated chambers become possible. Most of the recent designs for surface-diffraction

[17] W.C. Marra, PhD Thesis, Stevens Institute of Technology (1981).
[18] R. Feidenhans'l, PhD Thesis, Risø-M-Report 2569 (1986).
[19] S. Brennan and P. Eisenberger, *Nucl. Instr. and Meth.* **222**, 164 (1984).
[20] P.H. Fuoss and I.K. Robinson, *Nucl. Instr. and Meth.* **222**, 171 (1984).

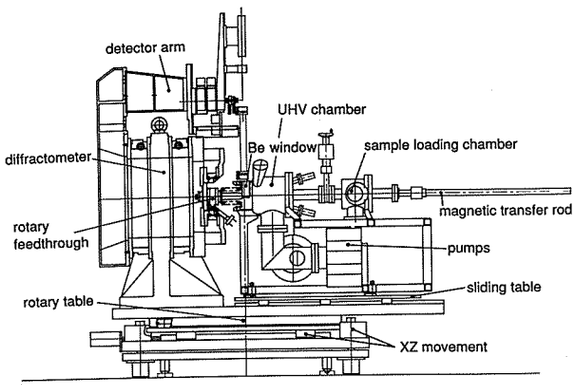

Fig. 10.3. A schematic of the setup of Vlieg et al. used at the synchrotron radiation source in Daresbury. Shown are the vacuum chamber connected to a 4-circle diffractometer via a rotary feedthrough. Everything is placed on top of a rotary table that makes the fifth degree of freedom.[21]

setups have used the concept of a rotary feedthrough. As an example, Fig. 10.3 shows the design of Vlieg et al.[21] This chamber is equipped with a sample-loading chamber, reflection high-energy electron diffraction (RHEED) and has facilities for MBE crystal growth during X-ray diffraction. The vacuum chamber is connected to a 5-circle diffractometer, whose degrees of freedom are shown schematically in Fig. 10.4.

In bulk crystallography one most often makes use of a 4-circle diffractometer. Because of the special constraints in the case of surface diffraction, it is advantageous to have more degrees of freedom available. In addition to the correct position (hk*l*) in reciprocal space, an important parameter in surface diffraction is the angle of incidence. In principle, four degrees of freedom are enough to fulfill these conditions, but this may lead to unfavourable sample orientations that deteriorate the resolution and that require special data correction factors.[22] Therefore, a 5- or 6-circle diffractometer is

[21] E. Vlieg, A. van 't Ent, A.P. de Jongh, H. Neerings and J.F. van der Veen, *Nucl. Instr. and Meth.* **A262**, 522 (1987).

[22] I.K. Robinson, *Aust. J. Phys.* **41**, 359 (1988).

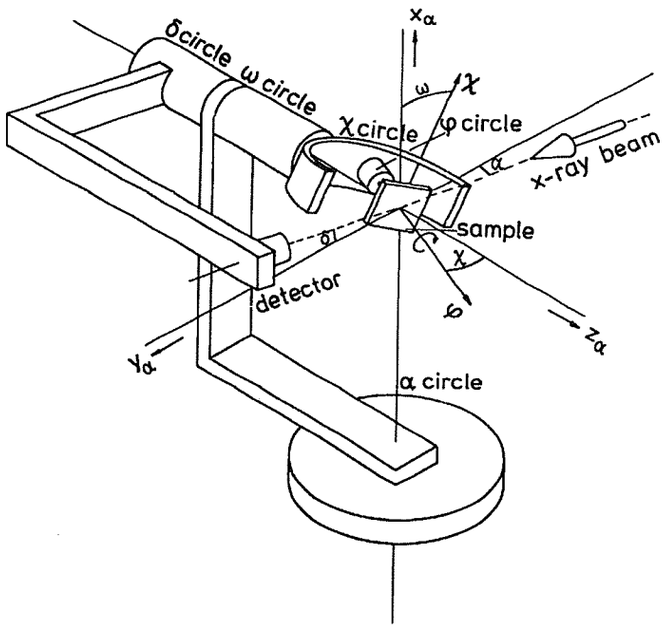

Fig. 10.4. Schematic of a 5-circle diffractometer showing the horizontally mounted 4-circle diffractometer on top of a rotary table. All circles are shown with a small positive setting.[23]

advantageous. With the 5-circle geometry shown in Fig. 10.4, the fifth degree of freedom can be used to set the surface normal always in the horizontal plane,[23] so that the rod-shaped diffraction intersects the narrow direction of the resolution function. An equally important advantage of the fifth degree of freedom is the increase in accessible reciprocal space along the out-of-plane direction as illustrated in Fig. 10.5.

Figure 10.5 also serves to illustrate the difference between the more conventional surface diffraction tool of low-energy electron diffraction (LEED) and X-ray diffraction using two types of diffractometers. LEED is primarily a backscattering technique, probing mainly perpendicular momentum transfer

[23] E. Vlieg, J.F. van der Veen, J.E. Macdonald and M. Miller, *J. Appl. Cryst.* **20**, 330 (1987).

(Fig. 10.5a). It is particularly sensitive to vertical displacements. Conversely, X-ray diffraction as most commonly practiced is a grazing-angle technique, with a correspondingly different subset (Fig. 10.5b) of the data sampled. The 4-circle (sample-tilting) geometry[24] is particularly restrictive for the inner reflections, when the tilting range is limited by the vacuum hardware. The extension to the 5-circle mode[23] has improved the situation significantly, as Fig. 10.5(c) shows. The incident beam can be inclined to a large angle relative to the surface, improving the range of perpendicular momentum transfer. This

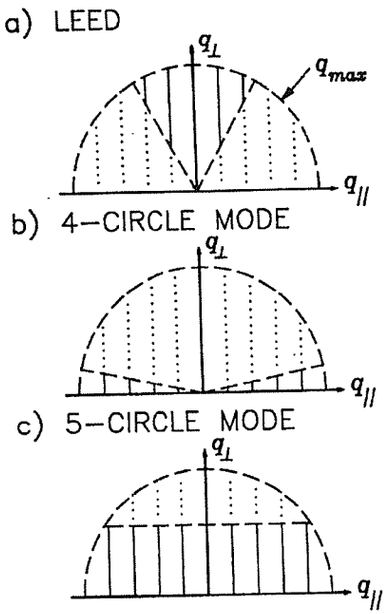

Fig. 10.5. Schematic reciprocal space diagrams showing the limited diffraction data available to LEED and two different X-ray diffraction configurations. The rods represent data, of which the solid parts are accessible. **q** is the momentum transfer. The hemispherical diffraction limit is an arbitrary total resolution cutoff at $|\mathbf{q}| = q_{max}$. (a) LEED. (b) 4-circle X-ray diffraction, assuming a maximum tilt angle of 11°. (c) 5-circle X-ray diffraction with a maximum inclination angle of 20°.[25]

24 I.K. Robinson, *Rev. Sci. Instrum.* **60**, 1541 (1989).
25 E. Vlieg, I.K. Robinson and K. Kern, *Surf. Sci.* **233**, 248 (1990).

is analogous to moving the detector out of plane[26]; the ability to do both is an anticipated further improvement.

10.5 Structure of Si(111)-($\sqrt{3}\times\sqrt{3}$)R30°-Ag

As an example of a structure determination by X-ray diffraction, we now discuss the ($\sqrt{3}\times\sqrt{3}$)R30° reconstruction of Si(111) induced by Ag adsorption. The term ($\sqrt{3}\times\sqrt{3}$)R30° means that the lattice parameters of the reconstructed surface unit cell are $\sqrt{3}$ times than the bulk ones, and that they are rotated by 30°. The example is only intended as an illustration; for a more detailed description of the experiment and a more extensive discussion of previous work the reader is referred to the literature.[27] Also the results shown may not be the final answer on the structure of this system, since work is still continuing.[28] The Ag-on-Si(111) system has been the subject of a large number of experimental and theoretical studies, but despite various proposed models, there is no consensus on the structure of this system. There is not even agreement on the number of Ag atoms present in the reconstructed surface unit cell.

As can be seen from the formula [10.27] for the structure factor, when data are taken at zero perpendicular momentum transfer ($l = 0$), the structure factor is insensitive to the z-coordinates of the atoms. In this manner the structure of the projected surface unit cell can be determined. This decoupling of in-plane and out-of-plane structure can greatly simplify a structure determination.

10.5.1 In-plane data

In the X-ray diffraction experiment 15 non-equivalent fractional-order reflections were measured at an l-value close to zero ($l = 0.1$). An example of an intensity profile is shown in Fig. 10.6. This profile is obtained by rotating

26 R. Feidenhans'l, *Surf. Sci. Rep.* **10**, 105 (1989).
27 E. Vlieg, A.W. Denier van der Gon, J.F. van der Veen, J.E. Macdonald and C. Norris, *Surf. Sci.* **209**, 100 (1989).
28 S. Kono, T. Abukawa, N. Nakamura and K. Anno, *Jpn J. Appl. Phys.* **28**, L1278 (1989); A. Ichimiya, S. Kohmoto, T. Fujii and Y. Horio, *Appl. Surf. Sci.* **41/42**, 82 (1989); E.L. Bullock, G.S. Herman, M. Yamada, D.J. Friedman and C.S. Fadley, *Phys. Rev.* **B41**, 1703 (1990); E. Vlieg, E. Fontes and J.R. Patel, *Phys. Rev.* **B43**, 7185 (1991).

the sample about the surface normal, while keeping the detector at a fixed angle. From the integrated intensity (the peak area) the structure factor is obtained after a few standard corrections, as given in [10.48].

The set of 15 reflections can be compared directly with a structure model by employing [10.17] to calculate theoretical structure factors and doing a least squares minimization on the variable parameters.[15] However, it turned out that none of the previously proposed models gave a satisfactory fit, all have χ^2-values in excess of 10. To help finding the correct structure, the Patterson function [10.56] was calculated from the experimental F_{hk0} values. The resulting contour plot is shown in Fig. 10.7. The Patterson map is biased since only fractional-order reflections were considered, but it can be shown that the maxima in such a Patterson map still give the positions of the interatomic vectors in the reconstructed unit cell.[29] If the atoms were to be on bulk positions, the interatomic vector would be vector **A**. We see, however, that new interatomic vectors appear. These are generated by displacing radially one group of three atoms outwards and another group of three atoms inwards. These two groups are labeled 2 and 3 in Fig. 10.7. If we assume the atoms in group 2 and 3 to be Ag and Si respectively, we obtain a substantially improved model for the projected unit cell ($\chi^2 = 3.5$). We find a displacement of 0.6 Å for Ag and 0.9 Å for Si. The χ^2 is reduced further to 1.82 if two Si atoms are added on positions 1. The latter atoms form a honeycomb when the unit cell is repeated. The χ^2-value finally drops to 1.34 if three additional Si atoms are introduced in the model. These atoms are radially displaced inward by a small amount (about 0.07 Å), with positions 2 as a starting point.

10.5.2 Rod scans

The x- and y-positions of the atoms in the unit cell are now known, but the corresponding z-positions are yet to be determined. The z-positions are found by measuring, for various fractional-order (hk) rods, $|F_{hkl}|$ as a function of l.

[29] J. Bohr, R. Feidenhans'l, M. Nielsen, M. Toney, R.L. Johnson and I.K. Robinson, *Phys. Rev. Lett.* **56**, 2878 (1986).

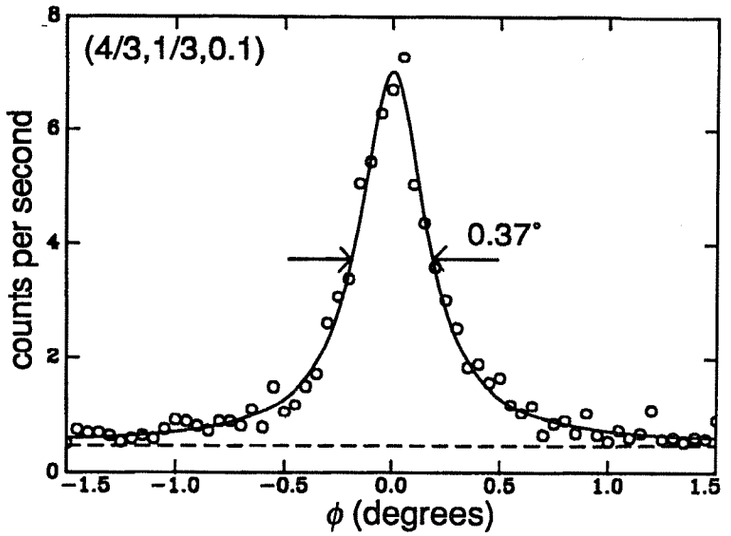

Fig. 10.6. A scan through the (4/3,1/3) reflection of Si(111)-($\sqrt{3}\times\sqrt{3}$)R30°-Ag (circles), where ϕ is the rotation angle of the sample. The solid curve is the fit to the data, using a Lorentzian profile and a constant background as indicated by the dashed line.

The results are shown in Fig. 10.8. The rod profiles can be fitted by using the projected surface unit cell as determined from the in-plane structure factors, and taking only the z-positions of the atoms as adjustable parameters. The best fit has a χ^2-value of 0.89, and is shown as the solid curves in Fig. 10.8.

Thus, with both types of data, a full structure determination has been accomplished, and the resulting model for the reconstructed surface is shown in Fig. 10.9. The $\sqrt{3}$ unit cell has three Ag atoms and a top layer of Si atoms that form a honeycomb. The Ag atoms are arranged in chained triangles, similar to what has been found in another X-ray diffraction analysis by Takahashi et al.[30] The Si atoms in the second layer are arranged in trimers that are almost coplanar with the Ag atoms. The Si atoms in the third layer are only slightly displaced from bulk lattice positions.

[30] T. Takahashi, S. Nakatani, N. Okamoto, T. Ishikawa and S. Kikuta, *Jpn J. Appl. Phys.* **27**, L753 (1988).

10.6 Summary of accomplishments in the field

We conclude this chapter with a brief list of references to accomplished work, having seen in detail a worked example of a surface crystallographic structure determination. The list is divided into semiconductor and metal surface structures, which will be handled separately. We shall group the results thematically rather than historically, and restrict the discussion to X-ray determinations only and to periodic structures. We also exclude results for step structures (under the general class of crystal morphology) or surface phase transitions that fall outside the scope of this chapter. Finally we defer discussion of all interfaces and non-vacuum surfaces.

10.6.1 Semiconductors

The simplest semiconductor surface structures, other than the ideal '1×1' bulk terminations that are rarely seen, are the $\sqrt{3}\times\sqrt{3}$ (111) family. The Ag-Si(111) surface we have already discussed is exceptionally complex, compared with the most commonly observed situation, where the adatom is located on top of a surface atom and has four nearest neighbors, a so-called T_4 site (Fig. 10.10). This represents the structure of Sn-Si(111),[31] Pb-Ge(111),[32-35] Bi-Si(111)[36,37] and Sn-Ge(111)[32,34,38] all at low coverage. In each case the induced strain leads to inward contraction of the immediate Si neighbours of the adatom. This results in perpendicular displacements in layers

[31] K.M. Conway, J.E. Macdonald, C. Norris, E. Vlieg and J.F. van der Veen, *Surf. Sci.* **215**, 555 (1989).
[32] J.S. Pedersen, R. Feidenhans'l, M. Nielsen, K. Kjaer, F. Grey and R.L. Johnson, *Surf. Sci.* **189/190**, 1047 (1987).
[33] F. Grey, PhD Thesis, Risø-M-Report 2737 (1988).
[34] J.S. Pedersen, PhD Thesis, Risø-M-Report 2713 (1988).
[35] R. Feidenhans'l, J.S. Pedersen, M. Nielsen, F. Grey and R.L. Johnson, *Surf. Sci.* **178**, 927 (1986).
[36] T. Takahashi, I. Takayama, T. Ishikawa, T. Ohta and S. Kikuta, *Jpn. J. Appl. Phys.* **24**, L727 (1985).
[37] T. Takahashi, S. Nakatani, I. Ishikawa and S. Kikuta, *Surf. Sci.* **191**, L825 (1987).
[38] J.S. Pedersen, R. Feidenhans'l, M. Nielsen, F. Grey and R.L. Johnson, *Phys. Rev.* **B38**, 13210 (1988).

2 and 3 (see Fig. 10.10), and consequently to *outward* relaxation of the three 4th-nearest neighbours in the 4th layer. The magnitudes of these lateral components are given in Table 10.1. The accuracy of the lateral components is

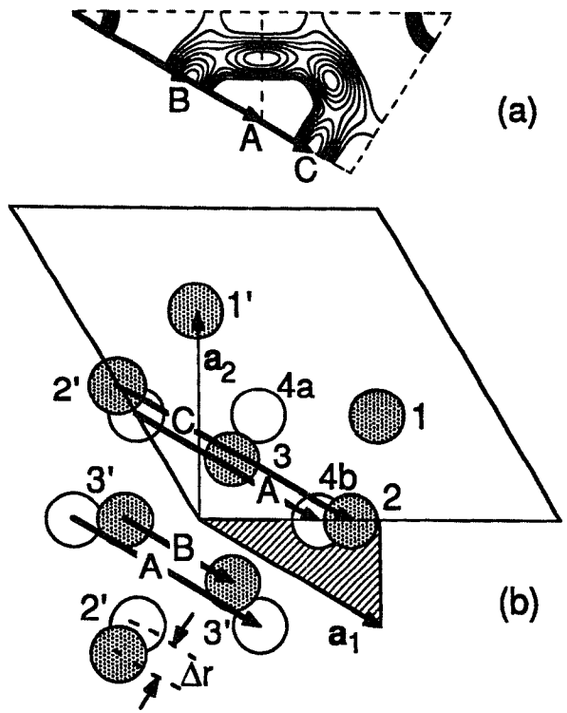

Fig. 10.7. (a) Contour plot of the Patterson function computed from the experimental fractional-order reflections for the Ag-Si(111) system. More than the irreducible unit (left triangle) is shown, in order to facilitate the interpretation. (b) Non-displaced positions in the (111) surface (hexagon of open circles) and the displaced positions in the reconstructed unit cell (dotted circles). The in-plane lattice vectors of the hexagonal unit cell are shown, together with an outline of the $\sqrt{3}$ unit cell. The hatched triangle indicates the irreducible unit of the Patterson function. The primed numbers indicate symmetry-equivalent positions. The displacements give rise to interatomic vectors **B** and **C**, which are visible in the Patterson function.

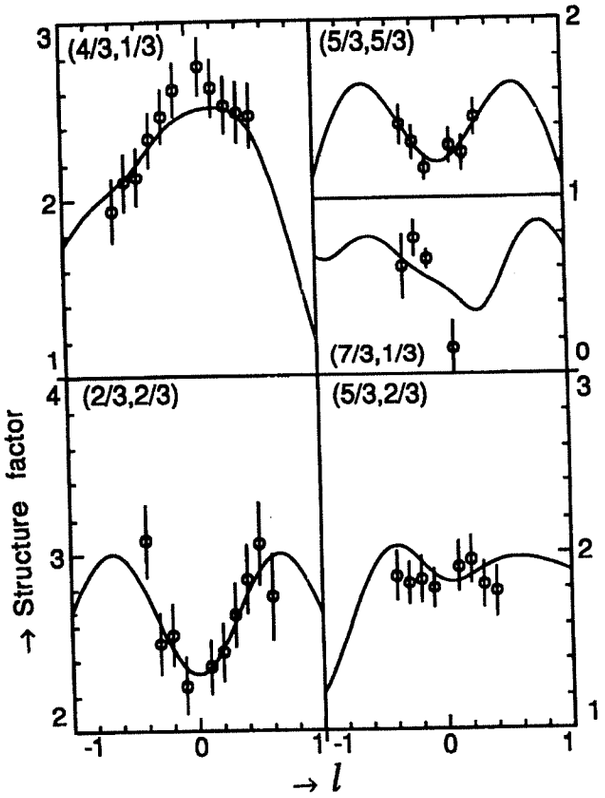

Fig. 10.8. Rod profiles for five different reflections measured on Ag-Si(111). Open circles are data points. The solid curves are the best fits.

always much better than for the perpendicular components, as will be discussed further below. The fits to rod-scan data for Sn-Ge(111) and Pb-Ge(111) are shown in Fig. 10.11, where the dramatic intensity modulations arising from the multilayer reconstruction can be seen clearly.

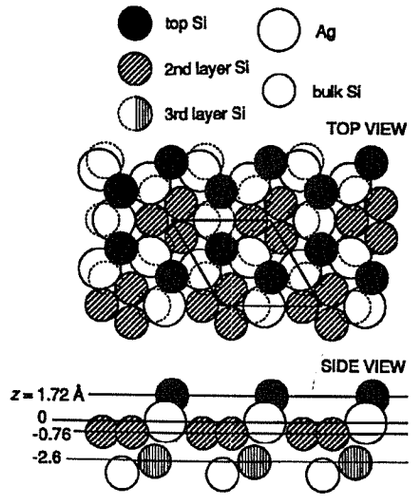

Fig. 10.9. The structure of the Si(111)-($\sqrt{3}$x$\sqrt{3}$)R30°-Ag reconstruction as determined by X-ray diffraction, with displacements drawn to scale. (a) Top view, with the $\sqrt{3}$ unit cell indicated. (b) Side view, with only the first few atoms shown for clarity.

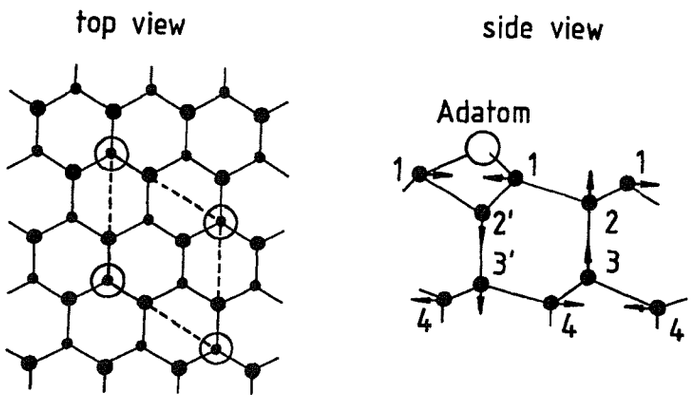

Fig. 10.10. Top and side views of the T_4 adatom site in a ($\sqrt{3}$x$\sqrt{3}$)R30° (111) semiconductor surface. Layers are numbered and the relaxations are denoted by arrows.

Table 10.1. In-plane displacements in adsorbate structures on Si(111) and Ge(111). Δr_1 and Δr_4 are displacements in the 1st and 4th layers of Fig. 10.10.

Surface	Δr_1 (Å)	Δr_4 (Å)	Ref.
Si(111) - Sn$\sqrt{3}$x$\sqrt{3}$	-0.12(2)	0.10(1)	[31]
Ge(111) - Sn$\sqrt{3}$x$\sqrt{3}$	-0.20(3)	0.11(1)	[32]
Ge(111) - Pb$\sqrt{3}$x$\sqrt{3}$	-0.16(3)	0.07(2)	[32]
Si(111) - B$\sqrt{3}$x$\sqrt{3}$	-0.26(2)	-0.02(1)	[40]

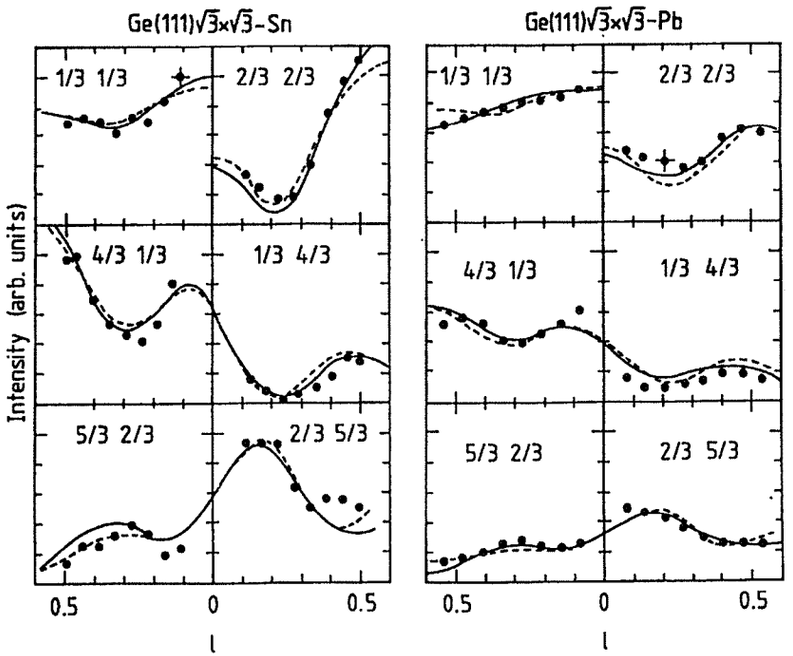

Fig. 10.11. Rod scan measurements (points) and fit to data (lines) using the 4-layer model of Fig. 10.10.

A striking exception is the B-Si(111) structure, listed in Table 10.1, for which the 4th-layer displacement is in the *opposite* sense and considerably smaller. This situation arises because the B atom occupies an altogether different site, where it is substitutional and has five nearest neighbors (S_5 site) (Fig. 10.12). Since the B-Si bondlength is around 15% shorter than Si-Si, this site is accommodated with less resulting strain than the T_4 site. It consequently results in very different behavior of this surface towards overgrowth of Si[39] and explains why a single layer of B can be largely retained at a Si/Si crystalline interface, while this situation in untenable with Ga for example.[40]

Higher densities of metals on semiconductors lead to a variety of different structures, including a second $\sqrt{3}\times\sqrt{3}$ phase of Pb-Ge(111) with a coverage of 4/3,[32-35] and incommensurate structures for Pb-Si(111)[41] and Au-Si(111).[42] In some cases these are close-packed structures where the commensurability is determined by the relative lattice parameters of the metal and semiconductor, just as it is in the well-studied noble gas/graphite systems.[43,44]

The T_4 adatom feature (Fig. 10.10) is a widely recurrent theme in more complex semiconductor surface structures. Indeed, its stability has been considered theoretically and it is found to be a very stable arrangement, both for metal adsorbates[45,46] and clean semiconductor (111) surfaces.[47] Part of this stability comes from backbonding of the adatom to the underlying atom, which reduces the total number of dangling bonds, and part from the relief of strain deep down. The backbond state has also been identified in inverse photoemission experiments, while the strain has been most clearly confirmed in the X-ray diffraction results summarized here.

---

39 R.L. Headrick, B.E. Wier, J. Bevk, B.S. Freer, D.J. Eaglesham and L.C. Feldman, *Phys. Rev. Lett.* **65** 1128 (1990).
40 R.L. Headrick, I.K. Robinson, E. Vlieg and L.C. Feldman, *Phys Rev. Lett.* **63** 1253 (1989).
41 F. Grey, R. Feidenhans'l, M. Nielsen, R.L. Johnson, *J. Phys. (Paris), Colloque* **C7**, 181 (1989).
42 R. Feidenhans'l, F. Grey, J. Bohr, M. Nielsen, R.L. Johnson, *J. Phys. (Paris), Colloque* **C7**, 175 (1989).
43 P.M. Horn, R.J. Birgeneau, P. Heiney and E.M. Hammonds, *Phys. Rev. Lett.* **41**, 961 (1978); J.P. McTague, J. Als-Nielsen, J. Bohr and M. Nielsen, *Phys. Rev.* **B25**, 7765 (1982).
44 K.L. D'Amico, D.E. Moncton, E.D. Specht, R.J. Birgeneau, S.E. Nagler and P.M. Horn, *Phys. Rev. Lett.* **53**, 2250 (1984).
45 J.E. Northrup, *Phys. Rev. Lett.* **53**, 683 (1984).
46 J.E. Northrup, *Phys. Rev. Lett.* **57**, 154 (1986).
47 D. Vanderbilt, *Phys. Rev.* **B36**, 6209 (1987).

The best-studied higher-order structures containing adatoms are the clean Ge(111)c(2×8) surface[48,49] and the famous Si(111)7×7[50–52] shown in Fig. 10.13. The 7×7 structure contains two independent T_4 adatoms in the unit cell, both of which demonstrate the lateral strain in the near-neighbor coordinates. The adatoms fit into an elegant network structure (Fig. 10.13) that has p6mm symmetry, while the ideal bulk has only p3m1 surface symmetry.

The extra mirror symmetry present in the surface layer, but not in the bulk, was observed directly in the diffraction pattern[53] and is an interesting exception to the normal rule that surface structures have lower symmetry than the bulk,

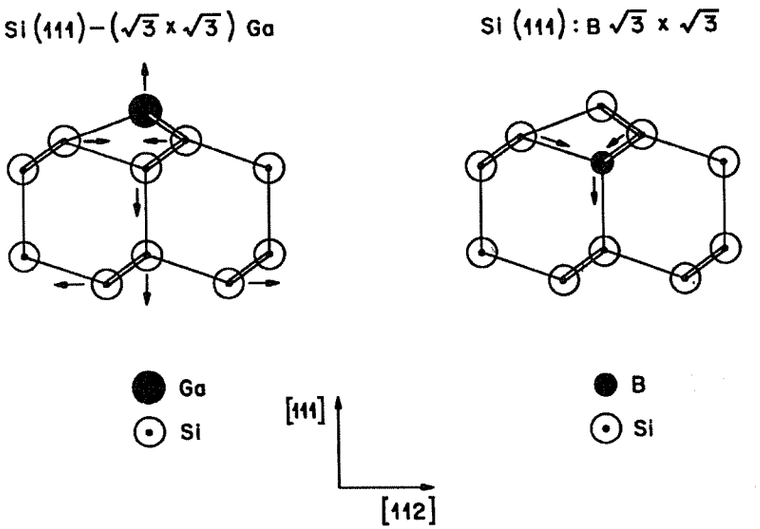

Fig. 10.12. The S_5 substitutional site of B-Si(111).

48 R. Feidenhans'l, J.S. Pedersen, J. Bohr, M. Nielsen, F. Grey and R.L. Johnson, *Phys. Rev.* **B38**, 9715 (1988).
49 R.G. van Silfhout, J.F. van der Veen, C. Norris and J.E. Macdonald, *Faraday Discuss. Chem. Soc.* **89**, 169 (1990).
50 K. Takayanagi, Y. Tanishiro, S. Takahashi and M. Takahashi, *Surf. Sci.* **164**, 367 (1985).
51 I.K. Robinson, W.K. Waskiewicz, P.H. Fuoss, J.B. Stark and P.A. Bennett, *Phys. Rev.* **B33**, 7013 (1986).
52 I.K. Robinson, W.K. Waskiewicz, P.H. Fuoss and L.J. Norton, *Phys. Rev.* **B37**, 4325 (1988).
53 I.K. Robinson, *Phys. Rev.* **B35**, 3910 (1987).

and thus contain twin domains.[54] Strain is central to the story of the stability of the 7×7 surface.[34,47,55,56] Ge(111) also forms both a 7×7 and a closely related 5×5 structure in the presence of Sn.[34,57] Here Sn, which lies immediately below Ge in the periodic table, acts to form a surface alloy since its occupation at the various sites in the structure appears to change with coverage. The order of phases for increasing Sn coverage on Ge(111) is $(\sqrt{3}\times\sqrt{3})R30°$, 7×7 then 5×5.[58] Even pure Ge(111) switches to the 7×7 structure when a moderate (1-2%) compressive strain is applied.[59]

Finally there are the InSb(111) and GaSb(111) surfaces, which give rise to 2×2 reconstructions.[29,60] Since these compounds are partially ionic and partially covalent in the bulk, they have new degrees of freedom available at their surfaces. The predominant driving mechanism for reconstruction appears to be charge neutralization, which changes the sp^3 outer electron shell of the bulk ions to s^2p^3 for Sb and to sp^2 for In and Ga. The sp^2 configuration corresponds to three 90° bonds (p orbitals) while the sp^2 configuration has three 120° bonds. The result is a structure with one quarter of the top layer metal atoms vacant, thereby reducing the surface dipole moment. The flat top layer arrangement gives rise to a strain field once again, evident in the pattern of small displacements seen in the second layer.[61]

If the T_4 adatom is the basic structural element of the semiconductor (111) surfaces then the *dimer* is the corresponding component of the (100) surfaces.

As shown in Fig. 10.14 the dimer functions primarily by halving the number of dangling bonds, but part of the stabilization energy lies in a strain field that,

54 F. Jona, J.A. Strozier, Jr. and W.S. Yang, *Rep. Progr. Phys.* **45**, 527 (1982).
55 I.K. Robinson, *J. Vac. Sci. Technol.* **A6**, 1966 (1988).
56 P.M.J. Marée, K. Nakagawa, J.F. van der Veen and R. M. Tromp, *Phys. Rev.* **B38**, 1585 (1988).
57 J.S. Pedersen. R. Feidenhans'l, M. Nielsen, F. Grey and R.L. Johnson, *Phys. Rev.* **B38**, 13210 (1988).
58 I. Ichikawa and S. Ino, *Surf. Sci.* **105**, 395 (1981).
59 H.J. Gossmann, J.C. Bean, L.C. Feldman, E.G. McRae and I.K. Robinson, *Phys. Rev. Lett.* **55**, 1106 (1985).
60 R. Feidenhans'l, M. Nielsen, F. Grey, R.L. Johnson and I.K. Robinson, *Surf. Sci.* **186**, 499 (1987).
61 I.K. Robinson, J. Bohr, R. Feidenhans'l, M. Nielsen, F. Grey, R.L. Johnson, *Surf. Sci.* **217**, L435 (1989).

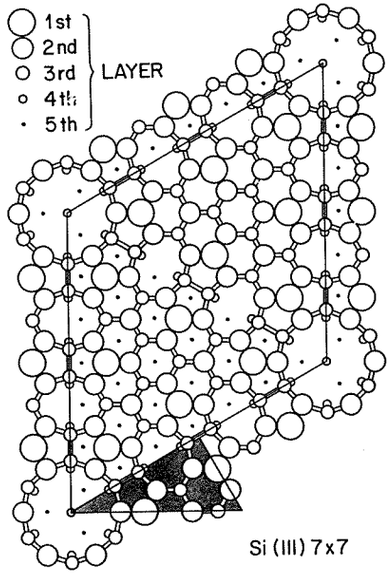

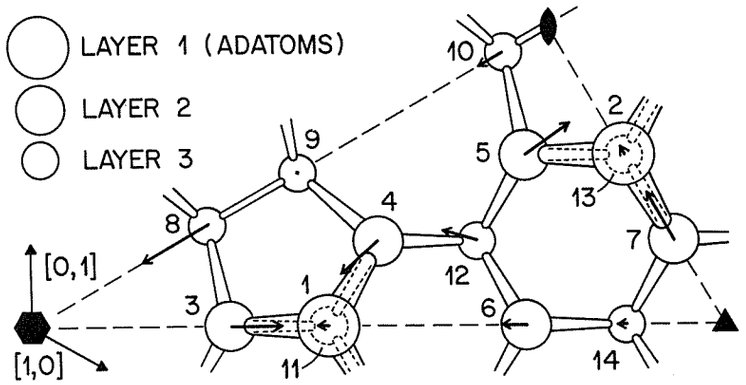

Fig. 10.13. The Dimer-Adatom-Stacking fault (DAS) model of Si(111)7×7.[50–52] The 7×7 contains two independent T_4 adatoms in the unit cell, showing lateral strain in the near-neighbor coordinates.

once again, penetrates very deep into the bulk, with displacement seen down to the 8th layer.[62,63] Both clean Ge(100) and Si(100) show the simple 2×1 dimer structures,[5,62,63] but the question of whether the dimer is symmetric or asymmetric is not at present resolved. GaAs(100) has a variety of different structures that depend on the surface stoichiometry, and therefore on the exact conditions of preparation: molecular beam epitaxy (MBE) is required to avoid the irreversible loss of As. The best studied surface is an As-rich phase that is a mixture of two structures of different stoichiometry (As coverage 0.5 and 0.75) but the same c-centered c(4×4) symmetry. These are both ordered As-dimer structures riding up on an As-terminated bulk.[64]

10.6.2 Metals

Whereas reconstructed surfaces are common for semiconductors, they are relatively uncommon for metals. Metal surfaces without reconstruction are accessible to X-ray diffraction through study of their CTRs but not much work of this kind has been undertaken to date. A few metal surfaces known to reconstruct, as well as adsorbate-induced reconstructions, have been studied.

W(100) has one of the simplest reconstructions that have so far been studied with X-rays.[65–67] As was previously known from LEED,[68] the surface has a zig-zag chain structure (Fig. 10.15), leading to additional coordination of the body-centered cubic (bcc) surface atoms. The aspect of this structure revealed by X-ray work was the presence of second layer displacements parallel to (and of order 20% the magnitude of) the outer layer displacements.[66]

---

62 F. Grey and R. Feidenhans'l, *Europhysics News* **19**, 94 (1988).
63 F. Grey, R.L. Johnson, J.S. Pedersen, R. Feidenhans'l and M. Nielsen, in *The Structure of Surfaces II*, J.F. van der Veen and M.A. van Hove, Eds., Heidelberg: Springer (1988), p. 292.
64 M. Sauvage-Simkin, R. Pinchaux, J. Massies, P. Claverie, N. Jedrecy, J. Bonnet and I.K. Robinson, *Phys. Rev. Lett.* **62**, 563 (1989).
65 J.W. Chung, K. Evans-Lutterodt, E.D. Specht, R.J. Birgeneau, P.J. Estrup and A.R. Kortan, *Phys. Rev. Lett.* **59**, 2192 (1987).
66 M.S. Altman, P.J. Estrup and I.K. Robinson, *Phys. Rev.* **B38**, 5211 (1988).
67 I.K. Robinson, M.S. Altman and P.J. Estrup, in *The Structure of Surfaces II*, J.F. van der Veen and M.A. van Hove, Eds., Heidelberg: Springer (1988). p. 157.
68 M. Debe and D. King, *Phys. Rev. Lett.* **39**, 708 (1977).

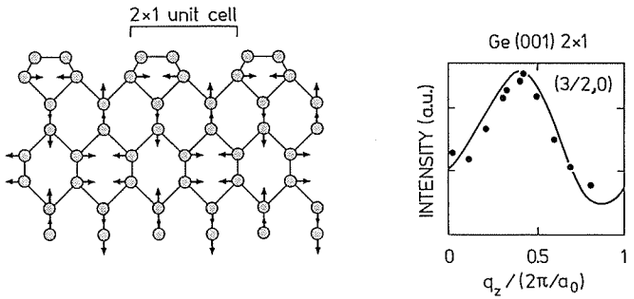

Fig. 10.14. The dimer functions in the Si(100) and Ge(100) surfaces by halving the number of dangling bonds. A strain field penetrates deep into the bulk.

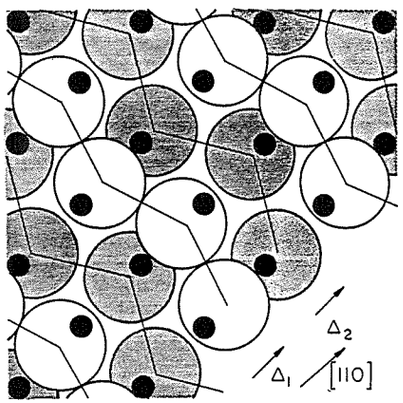

Fig. 10.15. Zig-zag chain reconstruction of W(100). The sites of the ideally terminated lattice are shown as dots. The atoms rearrange to form close-packed chains in the top layer (unshaded circles). Second-layer displacements (shaded) follow those of the top layer.

Au(110) and Pt(110) have a simple 'missing row' reconstruction shown in Fig. 10.16, again first studied with LEED.[69] This structure exposes (111) facets on the surface, which, due to relaxation of the coordinates, leads to a greater effective coordination of these atoms, and hence higher stability. Once

[69] W. Moritz and D. Wolf, *Surface Sci.* **163**, L655 (1985).

again, it was the application of X-ray crystallography to the problem that led to the discovery of large subsurface relaxations, including significant contributions from the 4th layer.[25,70] The two surfaces are also highly prone to formation of steps in which the facet edges extend by one row of atoms, and this leads to an interesting phase transition.[71] This is one of the most accurately known surface structures of all, and serves as a benchmark of precision in structure determination. Typical errors for X-ray crystallography are 0.01 Å parallel to the surface and 0.1 Å perpendicular,[25] while for LEED crystallography they are more like 0.1 Å parallel to the surface and 0.01 Å perpendicular.[72] The striking contrast arises from the different ranges of total momentum transfer typically used with the two techniques (see Fig. 10.5).[25,73] While the scattering vectors are nearly parallel to the surface in surface X-ray scattering, the geometry typical in LEED experiments corresponds to backscattering, with scattering vectors closer to the surface normal.

Au(100), Pt(100) and Au(111) all have hexagonal surface layers that are incommensurate with the rest of the crystal. Intermodulation effects that distort both the surface layer and the bulk are also clearly seen.[74–77]

Cu(100) and Cu(110) surfaces both reconstruct in the presence of oxygen to form missing-row structures,[78–80] different from those of Fig. 10.16 in the orientation of the rows deleted. The basic structural element here is a Cu-O-Cu-O-Cu chain along one of the in-plane crystallographic [100] directions. In this chemical environment the Cu apparently no longer needs as large a coordination

[70] I.K. Robinson, *Phys. Rev. Lett.* **50**, 1145 (1983).
[71] I.K. Robinson, E. Vlieg and K. Kern, *Phys. Rev. Lett.* **63**, 2578 (1989).
[72] P. Fery, W. Moritz and D. Wolf, *Phys. Rev.* **B38**, 7275 (1988).
[73] I.K. Robinson, E. Vlieg and K. Kern, *Faraday Discuss. Chem. Soc.* **89**, 159 (1990).
[74] L.D. Gibbs, B.M. Ocko, D.M. Zehner and S.G.J. Mochrie, *Phys. Rev.* **B38**, 7303 (1988).
[75] L.D. Gibbs, B.M. Ocko, D.M. Zehner and S.G.J. Mochrie, *Phys. Rev.* **B42**, 7330 (1990).
[76] B.M. Ocko, L.D. Gibbs, K.G. Huang, D.M. Zehner and S.G.J. Mochrie, *Phys. Rev.* **B44**, 6429 (1991).
[77] A.R. Sandy, S.G.J. Mochrie, D.M. Zehner, K.G. Huang and L.D. Gibbs, *Phys. Rev.* **B43**, 4667 (1991).
[78] K.S. Liang, P.H. Fuoss, G.J. Hughes and P. Eisenberger, in *The Structure of Surfaces I*, M.A. van Hove and S.Y. Tong, Eds., Berlin: Springer (1985), p. 246.
[79] R. Feidenhans'l, F. Grey, R.L. Johnson, S.G.J. Mochrie, J. Bohr and M. Nielsen, *Phys. Rev.* **B41**, 5420 (1990).
[80] I.K. Robinson, E. Vlieg and S. Ferrer, *Phys. Rev.* **B42**, 6954 (1990).

as in the bulk, and has fewer near neighbors in the plane. The Cu-O bondlength of 1.85 Å nicely matches half the 2nd-nearest-neighbour spacing of Cu along [100], 3.615 Å. The two structures are interrelated: the (110) can be considered to be made of 2-atom-wide strips of (100) and vice versa, as Fig. 10.17 shows. At higher coverages oxygen gives rise to a c(6×2) structure on Cu(110). This has also been analysed by surface X-ray crystallography to give the structure of Fig. 10.18: the extra oxygen is accommodated in a closer packing of Cu-O-Cu-O-Cu chains, 2 per 3 substrate unit cells, and also in O-Cu-O adatom arrangements.[81]

Metal-on-metal structures have been studied mainly in the context of phase transitions. Preliminary crystallographic analysis has been attempted to identify the phases concerned. Heavy metals such as Pb on Cu(100) have shown a series of structures.[82–84] Some clean metal surfaces not showing reconstruction have been examined at high temperatures to look for roughening or other phase transitions: Cu(110),[85,86] Cu(113),[87] Cu_3Au(100),[88] Ag(110)[89] and Ni(113).[90]

10.7 Future outlook

This chapter has demonstrated the principles of the techniques of surface X-ray diffraction and its application to surface crystallography. The steps involved in arriving at a structure were illustrated with one detailed example,

81 R. Feidenhans'l, F. Grey, M. Nielsen, F. Besenbacher, F. Jensen, E. Laegsgaard, I. Stensgaard, K.W. Jacobsen, J.K. Norskov and R.L. Johnson, *Phys. Rev. Lett.* **65**, 2027 (1990).
82 W.C. Marra, P.H. Fuoss and P M. Eisenberger, *Phys. Rev. Lett.* **49**, 1169 (1982).
83 S. Brennan, P.H. Fuoss and P.M. Eisenberger, *Phys. Rev.* **B33**, 3678 (1986).
84 K.S. Liang, K.L. D'Amico, C.H. Lee and E.Y. Sheu, to be published.
85 S.G.J. Mochrie, *Phys. Rev. Lett.* **59**, 304 (1987).
86 B.M. Ocko and S.G.J. Mochrie, *Phys. Rev.* **B38**, 7378 (1988).
87 K.S. Liang, E.B. Sirota, K.L. D'Amico, G.J. Hughes and S.K. Sinha, *Phys. Rev. Lett.* **59**, 2447 (1987).
88 H. Dosch, L. Mailander, A. Lied, J. Peisl, F. Grey, R.L. Johnson and S. Krummacher, *Phys. Rev. Lett.* **60**, 2382 (1988).
89 G.A. Held, J.L. Jordan-Sweet, P.M. Horn, A. Mak and R.J. Birgeneau. *Phys. Rev. Lett.* **59**, 2075 (1987).
90 I.K. Robinson, E.H. Conrad and D.S. Reed, *J. Phys. (Paris)* **51**, 41 (1990).

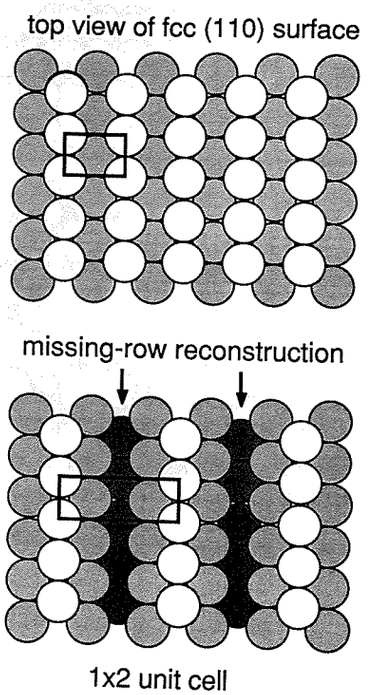

Fig. 10.16. Missing-row reconstruction of Au(110) and Pt(110).

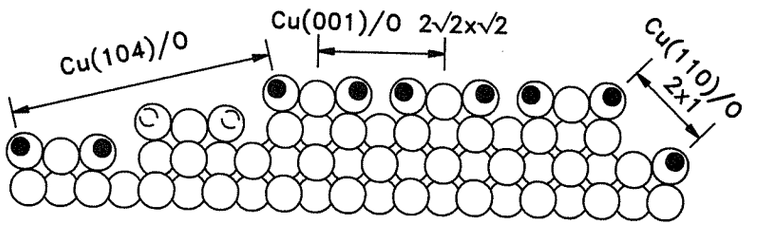

Fig. 10.17. Side view of the missing-row reconstructions of Cu(100)/O and Cu(110)/O. The similarity between these structures is evident. Both comprise Cu-O-Cu-O-Cu chains running perpendicular to the page.[74]

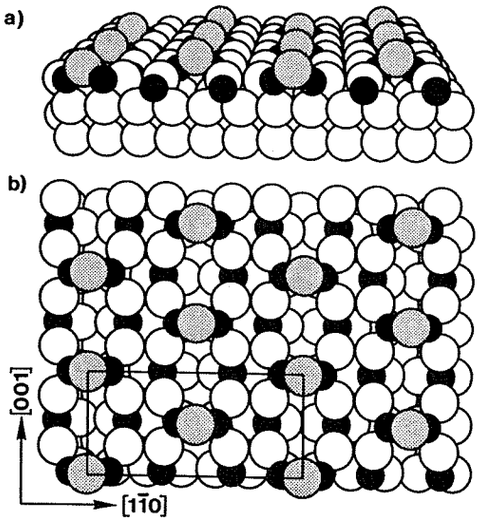

Fig. 10.18. Oblique and top views of the c(6×2) structure of Cu(110)/O, obtained with higher doses of oxygen. The density of Cu-O-Cu-O-Cu chains has increased and adatoms have appeared.[75]

from which the rigor of the technique should be apparent. This is because it relies heavily on that of its older brother, bulk X-ray crystallography. We have given a fairly complete list of surface structures determined with X-rays up to 1990.

In the future it is expected that surface X-ray diffraction will not only be applied to the interface between the surface and vacuum. Some work has been started on solid-liquid (electrochemical) interfaces showing induced reconstruction[91] and ordering during underpotential deposition.[92] A growing body of information pertains to solid-solid structures obtained by crystal growth: Ge on Ge,[93] $NiSi_2$ on Si(111),[94] amorphous Si on Si(111),[53,95]

[91] B.M. Ocko, J. Wang, A. Davenport and H. Isaacs, *Phys. Rev. Lett.* **65**, 1466 (1990).
[92] M.G. Samant, M.F. Toney, G.L. Borges, L. Blum and O.R. Melroy, *Surface Sci.* **193**, L29 (1987).
[93] E. Vlieg, A.W. Denier van der Gon, J.F. van der Veen, J.E. Macdonald and C. Norris, *Phys. Rev. Lett.* **61**, 2241 (1988).
[94] I.K. Robinson, R.T. Tung and R. Feidenhans'l, *Phys. Rev.* **B38**, 3632 (1988).

SiO_2 on Si(111),[95] SiO_2 on Si(100),[96] and buried reconstruction of GeSi(111)[97] and GaAs(100).[98] Since the experimental hardware requirements are less severe and no vacuum is required, this work should proceed on a wide front.

Finally, it should be mentioned that new third generation synchrotron sources, currently under development, are generally optimized for higher photon energies: 15–20 kV instead of 8–12 kV at present. The extra penetration of such X-rays will lead to a greater number of applications to buried interfaces.

[95] I.K. Robinson, W.K. Waskiewicz, R.T. Tung and J. Bohr, *Phys. Rev. Lett.* **57**, 2714 (1986).
[96] A. Ourmazd, P.H. Fuoss, J. Bevk and J.F. Morar, *Appl. Surf. Sci.* **41**, 365 (1989).
[97] K. Akimoto, J. Mizuki, T. Tatsumi, N. Aizaki and J. Matsui, *Surface Sci.* **183**, L297 (1987).
[98] J. Mizuki, K. Akimoto, I. Hirosawa, K. Hirose, T. Mizutani and J. Matsui, *J. Vacuum Sci. Technol.* **B6**, 31 (1988).